Targeted molecular-genetic imaging and ligand-directed therapy in aggressive variant prostate cancer

Fortunato Ferrara[a,b,1], Daniela I. Staquicini[a,b,1], Wouter H. P. Driessen[c,1], Sara D'Angelo[a,b], Andrey S. Dobroff[a,b], Marc Barry[a,d], Lesley C. Lomo[a,d], Fernanda I. Staquicini[a,b], Marina Cardó-Vila[a,b], Suren Soghomonyan[e], Mian M. Alauddin[f], Leo G. Flores II[f], Marco A. Arap[g], Richard C. Lauer[a,h], Paul Mathew[i], Eleni Efstathiou[c], Ana M. Aparicio[c], Patricia Troncoso[j], Nora M. Navone[c], Christopher J. Logothetis[c], Serena Marchiò[a,b,k,l], Juri G. Gelovani[e], Richard L. Sidman[m,2], Renata Pasqualini[a,b,2,3], and Wadih Arap[a,h,2,3]

[a]University of New Mexico Comprehensive Cancer Center, Albuquerque, NM 87131; [b]Division of Molecular Medicine, Department of Internal Medicine, University of New Mexico School of Medicine, Albuquerque, NM 87131; [c]David H. Koch Center, The University of Texas M. D. Anderson Cancer Center, Houston, TX 77030; [d]Department of Pathology, University of New Mexico School of Medicine, Albuquerque, NM 87131; [e]Department of Biomedical Engineering, Wayne State University, Detroit, MI 48201; [f]Department of Cancer Systems Imaging, The University of Texas M. D. Anderson Cancer Center, Houston, TX 77030; [g]Department of Urology, University of São Paulo Medical School, Sao Paulo 04604-006, Brazil; [h]Division of Hematology/Oncology, Department of Internal Medicine, University of New Mexico School of Medicine, Albuquerque, NM 87131; [i]Department of Hematology and Oncology, Tufts Medical Center, Boston, MA 02111; [j]Department of Pathology, The University of Texas M. D. Anderson Cancer Center, Houston, TX 77030; [k]Candiolo Cancer Institute-Fondazione del Piemonte per l'Oncologia, Istituto di Ricovero e Cura a Carattere Scientifico, Candiolo, Turin 10060, Italy; [l]Department of Oncology, University of Turin, Candiolo, Turin 10060, Italy; and [m]Department of Neurology, Beth Israel Deaconess Medical Center, Harvard Medical School, Boston, MA 02215

Contributed by Richard L. Sidman, September 17, 2016 (sent for review July 11, 2016); reviewed by Otis W. Brawley, Sanjiv S. Gambhir, and Bruce R. Zetter

Aggressive variant prostate cancers (AVPC) are a clinically defined group of tumors of heterogeneous morphologies, characterized by poor patient survival and for which limited diagnostic and treatment options are currently available. We show that the cell surface 78-kDa glucose-regulated protein (GRP78), a receptor that binds to phage-display-selected ligands, such as the SNTRVAP motif, is a candidate target in AVPC. We report the presence and accessibility of this receptor in clinical specimens from index patients. We also demonstrate that human AVPC cells displaying GRP78 on their surface could be effectively targeted both in vitro and in vivo by SNTRVAP, which also enabled specific delivery of siRNA species to tumor xenografts in mice. Finally, we evaluated ligand-directed strategies based on SNTRVAP-displaying adeno-associated virus/phage (AAVP) particles in mice bearing MDA-PCa-118b, a patient-derived xenograft (PDX) of castration-resistant prostate cancer bone metastasis that we exploited as a model of AVPC. For theranostic (a merging of the terms therapeutic and diagnostic) studies, GRP78-targeting AAVP particles served to deliver the human *Herpes simplex* virus thymidine kinase type-1 (*HSVtk*) gene, which has a dual function as a molecular-genetic sensor/reporter and a cell suicide-inducing transgene. We observed specific and simultaneous PET imaging and treatment of tumors in this preclinical model of AVPC. Our findings demonstrate the feasibility of GPR78-targeting, ligand-directed theranostics for translational applications in AVPC.

aggressive variant prostate cancer | ligand-directed theranostics | molecular imaging | gene therapy | AAVP

Prostate cancer, the most common carcinoma in men and a major cause of morbidity and mortality (1), is a clinically heterogenous disease. Although a majority of prostate cancers are highly responsive to androgen receptor (AR)-directed therapies, a subset is relatively resistant to these therapies and carries a dismal prognosis (2–5). At the extreme of this spectrum are the small-cell or neuroendocrine carcinomas, a predominantly AR-negative histological variant of the disease that is associated with atypical clinical features (such as visceral metastases, predominantly lytic bone metastases, low levels of prostate-specific antigen relative to tumor burden, bulky primary tumors, and high levels of lactic dehydrongenase and carcinoembryonic antigen) and responds to platinum-based chemotherapies (6). Although small-cell or neuroendocrine carcinomas of the prostate are rare at initial diagnosis, they are increasingly recognized in the castration-resistant phases of disease progression. Moreover, a larger group of morphologically heterogeneous prostate cancers share the clinical features of the small-cell neuroendocrine carcinomas and, likely, their underlying biology (7, 8); these have been grouped under the term aggressive variant prostate carcinomas (AVPC). The molecular underpinnings of the AVPC are likely shared with subsets of other

MEDICAL SCIENCES

Significance

Aggressive variant prostate cancer (AVPC) is a clinically defined tumor with neuroendocrine or small-cell differentiation, visceral metastases, low prostate-specific antigen, androgen receptor insensitivity, and poor/brief responses to androgen-deprivation or platinum-based chemotherapy. AVPC incidence has markedly increased, yielding an unmet diagnostic/therapeutic need. Here we adapted a patient-derived xenograft model and tumor samples to demonstrate ligand-directed theranostics of AVPC in vivo. We engineered human *Herpes simplex* virus thymidine kinase type-1 as a noninvasive imaging reporter/suicide transgene into adeno-associated virus/phage (AAVP) particles displaying motif ligands to cell surface-associated glucose-regulated protein 78kD (GRP78), toward a clinic-ready system. Although individual components of the AAVP system have been extensively investigated, this study is evidence of successful application in relevant preclinical models of untreatable and hard to diagnose aggressive tumor variants.

Author contributions: F.F., D.I.S., W.H.P.D., S.D., A.S.D., F.I.S., M.C.-V., R.L.S., R.P., and W.A. designed research; F.F., D.I.S., W.H.P.D., S.D., A.S.D., M.B., L.C.L., F.I.S., M.C.-V., S.S., and L.G.F. performed research; F.F., D.I.S., W.H.P.D., S.D., A.S.D., M.B., L.C.L., F.I.S., M.C.-V., S.S., M.M.A., L.G.F., M.A.A., S.M., R.L.S., R.P., and W.A. analyzed data; and F.F., S.D., A.S.D., M.A.A., R.C.L., P.M., E.E., A.M.A., P.T., N.M.N., C.J.L., S.M., J.G.G., R.L.S., R.P., and W.A. wrote the paper.

Reviewers: O.W.B., Emory University and American Cancer Society; S.S.G., Stanford University School of Medicine; and B.R.Z., Children's Hospital Boston and Harvard Medical School.

Conflict of interest statement: W.A. and R.P. are founders of AAVP BioSystems, which has licensed intellectual property related to the adeno-associated virus/phage (AAVP) technology, and they are inventors on patent applications and entitled to standard royalties if commercialization occurs. The University of Texas M. D. Anderson Cancer Center and the University of New Mexico Health Sciences Center currently manage these arrangements in accordance with their established institutional conflict of interest policy.

Freely available online through the PNAS open access option.

[1]F.F., D.I.S., and W.H.P.D. contributed equally to this work.

[2]To whom correspondence may be addressed. Email: richard_sidman@hms.harvard.edu, rpasqual@salud.unm.edu, or warap@salud.unm.edu.

[3]R.P. and W.A. contributed equally to this work.

This article contains supporting information online at www.pnas.org/lookup/suppl/doi:10.1073/pnas.1615400113/-/DCSupplemental.

epithelial tumors, such as the triple-negative breast cancers. However, molecular-imaging tools and specific therapeutic approaches tailored to the AVPC are lacking.

To evaluate potential "theranostic" (a merging of the terms therapeutic and diagnostic) strategies for AVPC, we exploited SNTRVAP, a peptide motif isolated by screening of combinatorial phage display libraries in the MDA-PCa-118b patient tumor-derived xenograft (PDX) in vivo (9, 10) (Fig. 1). SNTRVAP is a ligand to a functional supramolecular complex present on the cell surface and containing the 78-kDa glucose-regulated protein (GRP78), an endoplasmic reticulum chaperone involved in prosurvival mechanisms (11). Altered glucose metabolism of cancer cells, as well as glucose starvation in poorly vascularized tumors, are associated with GRP78 overexpression and translocation to the cell surface (12–14). Overexpression of GRP78 has been correlated with poor survival in patients with breast (15–17) and prostate cancer (10, 18–20). Its tumor-specific localization and stress-response attributes make cell surface GRP78 an attractive candidate receptor for ligand-directed strategies in solid tumor management (10, 21). Chimeric adeno-associated virus/phage (AAVP) particles (22–25) combine eukaryotic virus transduction efficiency to phage-targeting attributes. In this hybrid construct, the targeting agent (a ligand peptide) is expressed as a fusion within the phage pIII capsid protein, whereas the effector agent (a transgene) is inserted into the phage genome as a fully functional expression cassette under the control of a constitutive *CMV* promoter. Ligand-directed AAVP particles have been successfully evaluated in several preclinical transgenic and xenograft tumor-bearing mouse models, including carcinomas of the breast and prostate (22), soft-tissue sarcomas (26), and glioblastomas (27). Moreover, AAVP-mediated tumor vascular delivery of TNF has proven efficacy in human melanoma xenografts (28) and pancreatic neuroendocrine transgenic tumors (29), as well as in native tumors in dogs (30). Here we investigated the GRP78-targeting properties of SNTRVAP (10), exploiting its specific binding to cell surface GRP78 for tumor targeting in the MDA-PCa-118b PDX. SNTRVAP-directed, GRP78-targeting AAVP particles were used to deliver the human *Herpes Simplex* virus thymidine kinase type-1

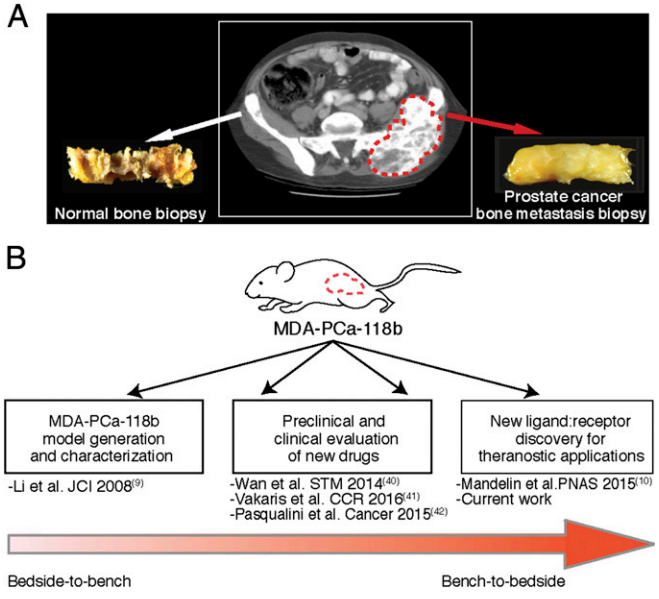

Fig. 1. Schematic representation of the MDA-PCa-118b PDX model generation and applications. (*A*) Index patient CT scan illustrating the original bone metastasis from which the MDA-PCa-118b PDX was obtained and propagated by subcutaneous injection in immunodeficient mice. (*B*) Sequential examples of translational research with this PDX model toward the present characterization of a ligand-directed theranostic approach for AVPC.

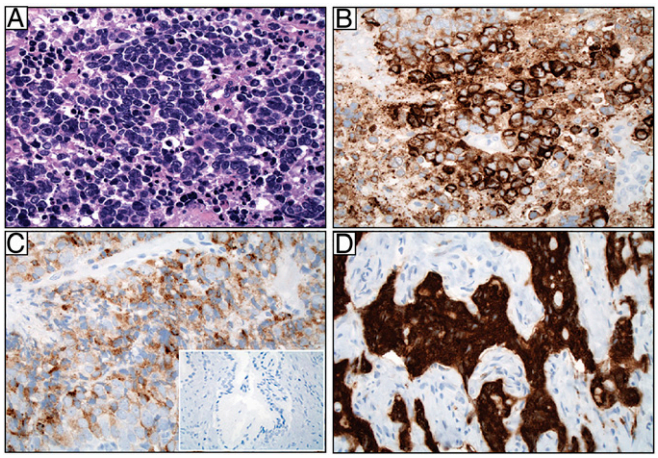

Fig. 2. GRP78 protein is expressed both in the cytoplasm and at the cell surface in AVPC specimens from patients. (*A*) Pathological evaluation of a representative specimen with high-grade cytology, small cell features, nuclear molding, and necrosis (H&E). (*B*) The same tumor stained for GRP78, moderate-to-strong (2–3+) intensity in tumor cells. (*C*) GRP78 staining of a representative case showing weak (1+) but diffuse positivity. (*D*) GRP78 staining of a representative case showing strong (3+) intensity. (*Inset*) Staining of normal prostate gland. (Magnification: *A–D*, 40×; *Inset*, 5×.)

(*HSVtk*) gene to act as both a noninvasive molecular-genetic imaging sensor/reporter, in the presence of a radiolabeled substrate, and a cell suicide-inducing transgene in the presence of ganciclovir (GCV), which is converted to a cytotoxic by *HSVtk*-expressing cells. This strategy proved to be effective as a targeted theranostic in preclinical models. GRP78-targeting AAVP particles are essentially "clinic-ready" for translation into urologic oncology.

Results

The Ligand Peptide SNTRVAP Targets Cell Surface GRP78 in AVPC. We first investigated the amount and localization of GRP78 in a pilot cohort of de-identified patients with primary small cell prostate carcinoma ($n = 4$). This initial analysis revealed a range from moderate-to-strong GRP78 immunostaining in both cytoplasm and cell surface in all patient-derived tumor samples examined (Fig. 2), a promising result in the light of translational applications. We next mapped the SNTRVAP:GRP78 interaction interface with an alanine-scanning site-directed mutagenesis approach (31). Phage particles displaying the parental SNTRVAP motif were compared with mutant particles in which each residue was individually converted to an alanine (or to glycine in the case of alanine itself in the parental motif) for binding to recombinant GRP78 in vitro. These assays showed that none of the residues were dispensable for the interaction: decreased binding to GRP78, ranging from partial (50–75%; site-directed mutagenesis of Ser^1, Thr^3, Arg^4, or Ala^6) to complete (>75%; site-directed mutagenesis of Asn^2, Val^5, or Pro^7) inhibition was observed for all mutants compared with the parental motif (Fig. 3*A*). These results are consistent with the concept that a three-residue motif in the primary structure is necessary and sufficient for peptide-protein recognition (32). SNTRVAP specificity was further validated in DU145, a human prostate cancer-derived cell line developed from a brain metastases—which is AR-negative—Tp53 and p16 mutant, and results in lytic bone metastases when implanted in mice, all features that overlap with clinical and molecular features of AVPC (7, 8). Importantly, these cells express high levels of GRP78, and are therefore a suitable model for ligand-directed approaches. To obtain an internal control for specificity, GRP78 was silenced by small-hairpin RNA (shRNA). We observed that two of five GRP78 shRNA vectors (i.e., clones #3 and #5) effectively down-modulated GRP78 (Fig. 3*B*), and consequently led to a

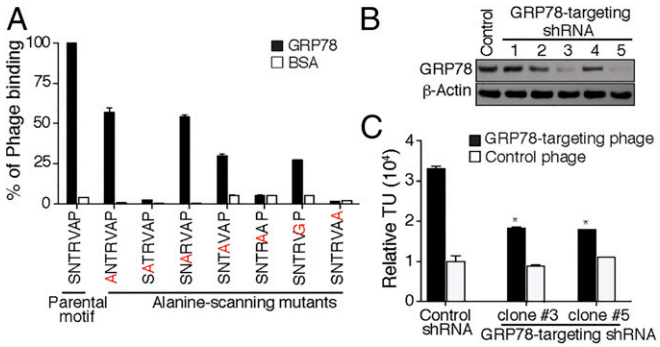

Fig. 3. In vitro validation of SNTRVAP and GRP78 as a ligand-receptor. (*A*) Ala-scanning site-directed mutagenesis of SNTRVAP. Each residue in the SNTRVAP sequence was mutated and the resulting phage particles were tested for binding to recombinant GRP78. Results are shown after normalization as the mean ± SEM in triplicate wells. (*B*) In vitro GRP78 silencing. DU145 cells were infected with lentiviral vectors expressing different GRP78 shRNA constructs, and GRP78 levels were assessed by Western blot. β-Actin served as a loading control. (*C*) The GRP78-targeting phage specifically binds to DU145 cells expressing cell surface GRP78. Binding is shown as transducing units (TU) relative to the control phage, $*P < 0.05$ by two-tailed Student's *t* test.

commensurate decrease in cell surface binding of GRP78 to SNTRVAP-displaying phage particles (Fig. 3*C*) ($P < 0.05$ by two-tailed Student's *t* test). Taken together, these results confirm a specific interaction between the SNTRVAP and GRP78, and support the possibility of exploiting this ligand-receptor in AVPC.

SNTRVAP Targets GRP78-Expressing Tumor Xenograft Models in Vivo. We next validated the targeting efficacy of SNTRVAP in immunodeficient mice implanted with either parental or GRP78-silenced DU145 tumor cells. Differential GRP78 expression levels in tumor xenografts were confirmed by immunohistochemistry (IHC) (Fig. 4*A*) and quantification of specific signals (Fig. 4*B*). GRP78-targeting or control phage particles were administered intravenously into DU145-derived tumor-bearing mice, and phage particle localization was evaluated after 24 h by staining with an antiphage antibody (33) (Fig. 4*C*), followed by quantification of DAB signals (Fig. 4*D*) and titration of phage particles by quantitative PCR (qPCR) (34) (Fig. 4*E*). The GRP78-targeting phage particles localized in parental DU145-derived tumors but not in size-matched GRP78-silenced DU145-derived tumors. Regardless of cell surface GRP78 levels, control phage particles did not accumulate in tumor xenografts. GRP78-targeting or control phage particles were present in the liver because of the long-recognized virus retention by the reticuloendothelial system (35–37), whereas neither was detectable in control tissues. Taken together, these results establish that the ligand peptide SNTRVAP targets AVPC-like cells that express cell surface GRP78 in vivo.

Targeting Cell Surface GRP78-Expressing Cells for in Vitro and in Vivo Small-Interfering RNA Delivery. As another step toward potential applications of the GRP78-targeting peptide motif, we explored the possibility of delivering small-interfering RNA (siRNA) and shRNA species to tumors that express cell surface GRP78. Transduction of parental GRP78-expressing DU145 cells was first evaluated in vitro with a custom GAPDH-specific siRNA conjugated to the GRP78-targeting peptide SNTRVAP, in comparison with GAPDH-specific siRNA administered by a standard transfection system (NeoFX). Quantification of GAPDH mRNA showed that the GRP78-targeting system is twice as effective as the standard reference. Equimolar concentrations of either an unconjugated GAPDH siRNA or a GRP78-targeting control siRNA were ineffective, further supporting the ligand-receptor specificity (Fig. 5*A*). We next coupled the GRP78-targeting peptide to a GRP78 siRNA sequence (Fig. 5*B*). The efficacy of this GRP78-targeting GRP78 siRNA was evaluated in vivo in comparison with a control unconjugated siRNA. Forty-eight hours after siRNA administration into DU145 tumor-bearing mice, either GRP78-targeting or control phage particles were administered intravenously and allowed to circulate for 24 h, followed by tumor collection. Quantification of tumor-retrieved phage particles revealed an inhibition (>40%) of GRP78-targeting particles

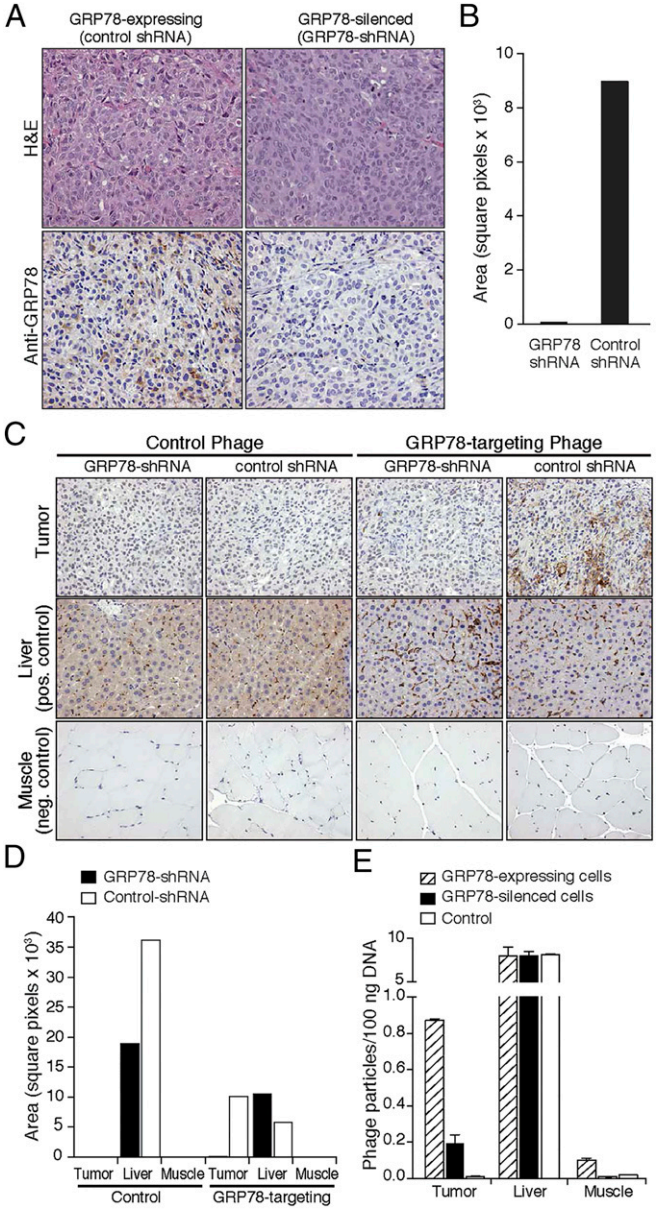

Fig. 4. In vivo validation of SNTRVAP and GRP78 as a ligand-receptor. (*A*) Animal models of GRP78-expressing and -silenced AVPC. DU145 cells transduced with control or GRP78 shRNA were injected subcutaneous into the flank of athymic BALB/c mice and tumors were grown for 6–8 wk. H&E staining (*Upper*) and GRP78 IHC (*Lower*) are shown. (*B*) Quantification of GRP78 staining was obtained by deconvolution with ImageJ and is expressed as number of pixels per optical field. (*C*) In vivo accumulation of GRP78-targeting phage. Phage localization was evaluated on excised tumor masses by IHC. Liver and muscle were used as control organs. (*D*) Quantification of IHC signals was obtained as in *B*. (*E*) Phage DNA was extracted and quantified by qPCR. Numbers of phage particles per 100 ng of total DNA are represented as mean ± SEM. Magnification in *A* and *C* is 20×.

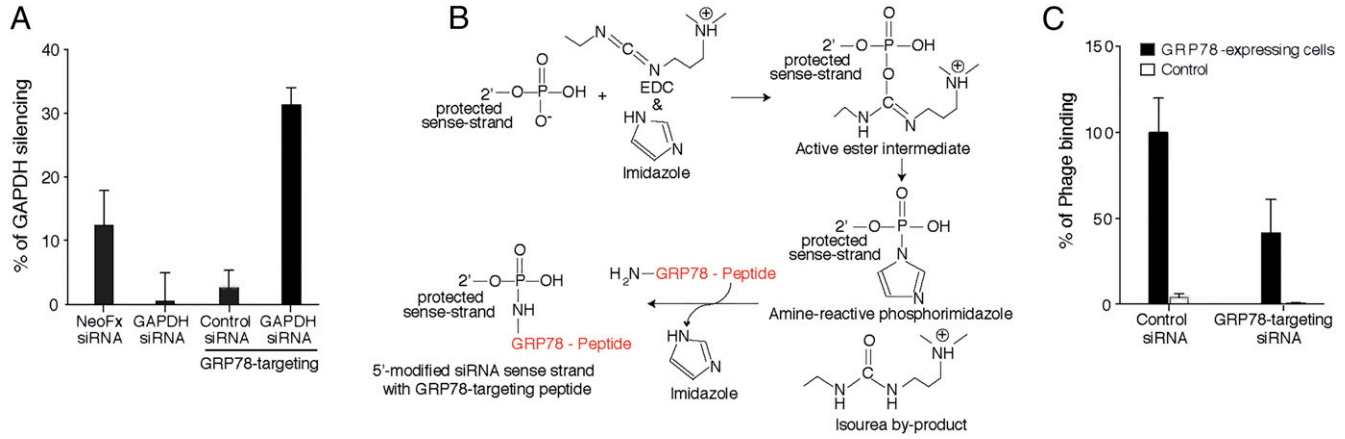

Fig. 5. In vitro and in vivo ligand-directed silencing of GRP78. (*A*) The GRP78-targeting peptide, chemically conjugated to a GAPDH siRNA, was incubated with GRP78-expressing DU145 cells followed by evaluation of GAPDH mRNA levels. GAPDH siRNA transfection with NeoFX was used as a standard. An unrelated siRNA and an unconjugated GRP78-targeting peptide were used as controls. Values are expressed as percent silencing of GAPDH. (*B*) Conjugation scheme of GRP78-targeting peptide to the 5′-modified GRP78 sense-strand siRNA. (*C*) GRP78-targeting siRNA or control siRNA were injected intravenously into DU145 tumor-bearing mice 48 h before intravenous injection of either untargeted or GRP78-targeting phage. After 24 h, tumors were excised and phage was quantified by bacterial infection. Values are expressed as percent accumulation compared with GRP78-targeting phage on nonsilenced cells, and are shown as mean ± SEM of three experiments.

in tumor-bearing mice pretreated with GRP78-targeting GRP78-siRNA, compared with the control siRNA. Finally, the corresponding control particles were not detected in tumors of treated mice (Fig. 5*C*). These results demonstrate that the SNTRVAP can target a GRP78-specific siRNA and effectively down-modulate GRP78 on AVPC cells in vivo.

SNTRVAP Mediates GRP78 Targeting for Transgene Delivery to a PDX Model. Having confirmed the efficacy and specificity of GRP78 targeting via the ligand peptide SNTRVAP in vitro and in vivo, we evaluated the efficacy of GRP78-targeting AAVP particles for in vivo genetic transduction of GRP78-expressing tumors (22). As mentioned above, the *HSVtk* gene product (thymidine kinase) functions as (*i*) an imaging tool in the presence of a radiolabeled substrate, and (*ii*) a cell suicide-inducing transgene in the presence of GCV (38). We evaluated both functions toward theranostic anti-AVPC strategies. Mice bearing the MDA-PCa-118b PDX model were randomized into four cohorts receiving: (cohort 1) control AAVP plus saline; (cohort 2) GRP78-targeting AAVP plus saline; (cohort 3) control AAVP plus GCV; (cohort 4) GRP78-targeting AAVP plus GCV. Daily treatments with either saline or GCV were started 5 d after intravenous administration of AAVP particles, as indicated, and continued for 7 d. Twenty-four hours after the last treatment, mice received [^{18}F]-fluorodeoxyglucose ([^{18}F]-FDG) to assess tumor viability as a function of glucose metabolism by PET/CT. Expression of the *HSVtk* transgene was evaluated after another 24 h by PET immediately after intravenous administration of 2-[^{18}F]-fluoro-2-deoxy-1-D-arabinofuranosyl-5-ethyluracil ([^{18}F]-FEAU) (26, 39). (See *Supplemental Discussion: Comparison Between the [^{18}F]-FEAU and ^{124}I-FIAU Substrates* for more on the [^{18}F]-FEAU substrate). Cohorts 1 and 2 were evaluated in protocols for ligand-directed molecular-genetic imaging. In these PDX-bearing mice, GRP78-targeting AAVP particles specifically localized at sites superimposable with metabolically active tumors, as visualized by [^{18}F]-FDG PET/CT scans, whereas the control AAVP particles did not show specific accumulation (Fig. 6*A*). Nonspecific localization of both [^{18}F]-FDG and [^{18}F]-FEAU in the kidneys and urinary bladder was observed in all cohorts as a result of renal clearance. Quantification of [^{18}F]-FEAU (represented here as percentage of the [^{18}F]-FEAU dose administered) confirmed that *HSVtk* tumor expression in mice receiving GRP78-targeting AAVP particles was significantly higher than in mice receiving control AAVP particles ($P < 0.001$ by two-tailed Student's *t* test) (Fig. 6*B*). PDX-bearing mouse cohorts 3 and 4 were evaluated in protocols for ligand-directed therapy. PET/CT scans demonstrated decreased tumor size in GRP78-targeting AAVP-administered mice treated with GCV, compared with the control AAVP plus GCV (Fig. 6*C*). This inhibition of tumor growth in PDX-bearing mice treated with GRP78-targeting AAVP plus GCV was independently confirmed by measuring gross tumor sizes with calipers, which revealed an average 50% reduction in tumor size ($P < 0.001$ by two-tailed Student's *t* test) (Fig. 6*D*). Excised tumors were also subjected to microtomography to quantify the percentage of mineralized tissue, a typical feature of osteoblastic metastases from prostate cancer. The growth of densely mineralized bone was significantly suppressed in animals treated with GRP78-targeting AAVP plus GCV, compared with treatments with GRP78-targeting AAVP plus saline or control AAVP ($P < 0.05$ by 2-way ANOVA followed by Bonferroni's test) (Fig. 7*A*). PDX tumors from mice treated with GRP78-targeting AAVP plus GCV were highly apoptotic as visualized by TUNEL staining, as opposed to tumors in mice treated with either GRP78-targeting AAVP plus GCV or control AAVP (Fig. 7*B*). These data were confirmed by the quantification of specific IHC signals (Fig. 7*C*). These results demonstrate the efficacy of the peptide SNTRVAP for ligand-directed strategies that target GRP78 as a cell surface receptor in a clinically-relevant model of AVPC.

Discussion

The combination of improved management and longevity of prostate cancer patients, along with increasing awareness of AVPC (7, 8), has led to a need for more specific tools for detection and treatment of this aggressive phenotype. Given that patients with AVPC are relatively insensitive to AR-directed therapies, and respond only transiently to chemotherapy (2–8), the development of a strategy that would work across molecular and cellular diversity in AVPC remains an unmet need. New technological approaches, such as the emerging field of theranostics, may prove useful to enable biopsy-free spatiotemporal tumor monitoring. As a proof-of-concept for serial ligand-directed theranostics, we herein provide preclinical applications of simultaneous noninvasive molecular-genetic imaging and therapy of AVPC based on targeting the tumor cell surface receptor GRP78.

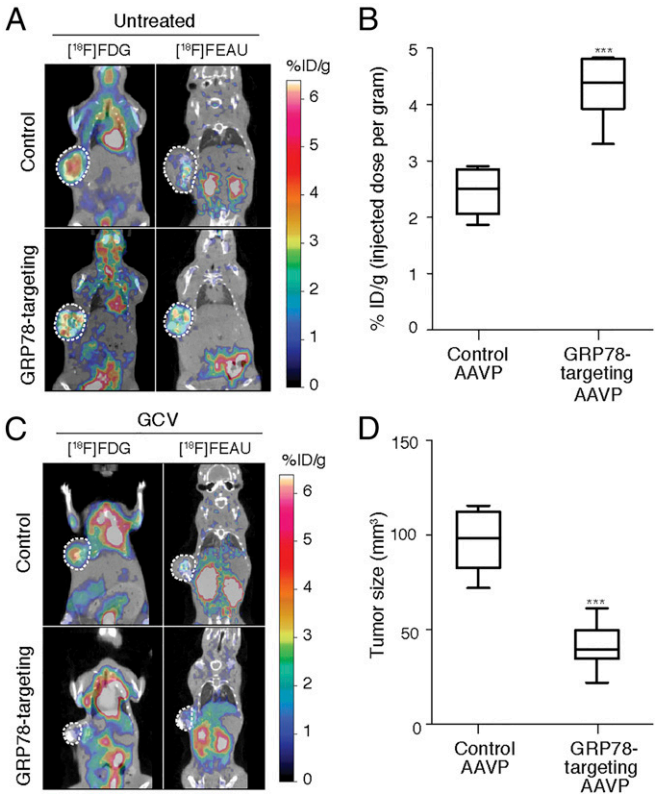

Fig. 6. Ligand-directed theranostics of the MDA-PCa-118 PDX model. (*A*) PET/CT imaging of MDA-PCa-118b PDX-bearing mice administered intravenously with GRP78-targeting or control AAVP. The pseudocolor scale represents signal intensity of [^{18}F]-FDG (metabolic activity) or [^{18}F]-FEAU (*HSVtk* activity). ***$P < 0.001$ by two-tailed Student's *t* test. (*B*) Quantification of *HSVtk* gene expression by micro-PET imaging of [^{18}F]-FEAU substrate. ***$P < 0.001$ by two-tailed Student's *t* test. (*C*) PET/CT imaging of MDA-PCa-118b PDX-bearing mice administered as in *A*, and 7 d later treated with GCV for 5 d. (*D*) Tumor sizes were assessed by caliper measurement. ***$P <$ 0.01 by two-way ANOVA followed by Bonferroni's test.

The MDA-PCa-118b PDX used in this work was unique in being a fully characterized in vivo model of osteogenic prostate cancer (9), and it has subsequently been used to unveil molecular mechanisms in metastatic tumors of the prostate (10, 40–42). The MDA-PCa-118b PDX is both castration-resistant and capable of developing soft-tissue and osteogenic tumors in mice (9), indicating that it is indeed representative of the highly aggressive pathology spectrum of AVPC; therefore, one may assume that the inherent mechanisms of disease progression, experimental findings, and targeting concepts uncovered by using the MDA-PCa-118b PDX are generalizable to the large "universe" of AVPC patients. By in vivo selection of phage-display random peptide libraries in the MDA-PCa-118b PDX, we have recently identified SNTRVAP as a highly specific ligand to GRP78 on the surface of cells within and adjacent to bone-like tumors (10). GRP78 up-regulation and relocation to tumor cell surface are associated with aggressive growth and invasive properties, and have been previously reported in human cancer cell lines and tissues (12). In prostate cancer, GRP78 expression levels correlate with the development of a metastatic disease in which circulating anti-GRP78 auto-antibodies are indicative of poor survival (21, 43). These observations support a potential translation of GRP78-based theranostics for the management of AVPC, including the widespread metastatic burden that remains a major clinical feature of AVPC patients (7, 8, 44). Additional GRP78-binding sequences, such as Trp-rich peptide motifs, have been reported (21, 45). Among these peptides, WIFPWIQL targets cell surface GRP78 in tumor-bearing mice and in human specimens of prostate cancer (10, 21, 22). Similar applications of this peptide are reported in our companion article on aggressive variants of breast cancer (46). Here, we chose the peptide SNTRVAP (10) to target AVPC for several reasons: (*i*) its original selection in the MDA-PCa-118b PDX itself; (*ii*) its selectivity for a prostate cancer-specific cell surface supramolecular complex that incorporates GRP78, prostate-specific antigen, and α2 microglobulin (10, 47); (*iii*) its ability to bind AVPC cells either per se or loop-grafted into an antibody backbone; and (*iv*) its superior hydrosolubility relative to the GRP78-binding Trp-rich motifs, which generally harbingers cost-effective production yields in aqueous formulations.

Our studies validate the application of GRP78-targeting AAVP particles as molecular-genetic imaging tools for PET/CT applications, in agreement with the increased expression of cell surface GRP78 during metastatic progression and, in general, in the most aggressive castration-resistant forms of prostate cancer collectively included in the broad definition of AVPC (7, 8). Besides staging and active surveillance of prostate cancer during treatment, such a biomarker-annotated theranostic strategy is expected to provide specific ligand-directed detection of biochemical relapse: that is, to reveal the earliest possible recurrence of GRP78^{+} tumor cells.

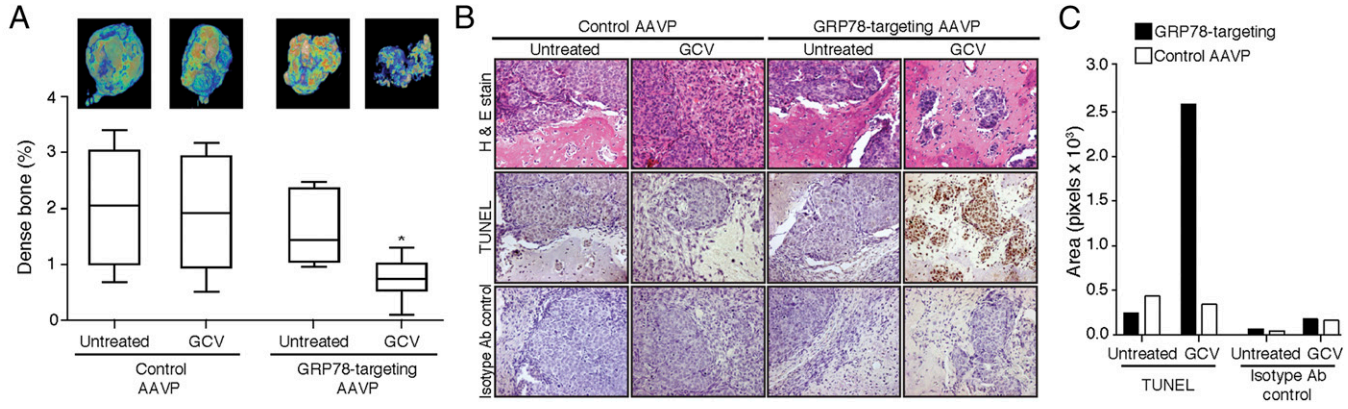

Fig. 7. GRP78-targeting AAVP particles reduce bone density and induce apoptosis in GCV-treated MDA-PCa-118b PDX models. (*A*) Evaluation of bone density of implanted tumors. (*B*) H&E staining and TUNEL assays were performed on MDA-PCa-118b tumor sections from mice administered intravenously with control or GRP78-targeting AAVP particles, and treated with saline or GCV. Control, secondary antibody only. (Magnification: 20×.) (*C*) DAB signals were isolated by deconvolution and quantified with ImageJ, and are represented as number of pixels per optical field. *$P < 0.05$ by two-way ANOVA followed by Bonferroni's test.

Remarkably, this theranostic tool enables simultaneous therapeutic options that address the composite disease burden in valuable models of human AVPC. In summary, GRP78-targeting AAVP particles provide an efficient approach to address preclinical models of human AVPC for imaging and therapy and, as such, should be considered for translation into clinical applications in patients with this aggressive disease phenotype. Given that AVPC patients share complex genetic and epigenetic lesions (48), AAVP-based transcriptomic reporter analysis of promoter-mediated gene expression may be incorporated into the ligand-directed theranostic approach introduced here.

Materials and Methods

The use of human samples has been reviewed and approved by the Clinical Ethics Service, Institutional Biohazard Committee, Clinical Research Committee, and Institutional Review Board of the University of New Mexico Comprehensive Cancer Center. The animal experiments were reviewed and approved by the Institutional Animal Care and Utilization Committee of M. D. Anderson Cancer Center. Reagents and all experimental procedures, such as the design of targeted AAVP and all in vivo and in vitro applications, are fully described in *SI Materials and Methods*.

ACKNOWLEDGMENTS. We thank Dr. Andrew R. Bradbury (Los Alamos National Laboratory) for critical reading of the manuscript, and Dr. Helen Pickersgill (Life Science Editors) for editorial services. This work was supported in part by Department of Defense IMPACT Grant W81XWH-09-1-0224; award funding from AngelWorks and the Gillson-Longenbaugh Foundation (all to W.A. and R.P.); Cancer Center Support Grant P30 CA016672 of the National Cancer Institute to the University of Texas M. D. Anderson Cancer Center and Grant P30 CA118100 to the University of New Mexico Comprehensive Cancer Center (to W.A. and R.P.).

1. Siegel RL, Miller KD, Jemal A (2015) Cancer statistics, 2015. *CA Cancer J Clin* 65(1):5–29.
2. Hussain M, et al.; Southwest Oncology Group Trial 9346 (INT-0162) (2006) Absolute prostate-specific antigen value after androgen deprivation is a strong independent predictor of survival in new metastatic prostate cancer: data from Southwest Oncology Group Trial 9346 (INT-0162). *J Clin Oncol* 24(24):3984–3990.
3. Efstathiou E, et al. (2012) Effects of abiraterone acetate on androgen signaling in castrate-resistant prostate cancer in bone. *J Clin Oncol* 30(6):637–643.
4. Ryan CJ, et al.; COU-AA-302 Investigators (2013) Abiraterone in metastatic prostate cancer without previous chemotherapy. *N Engl J Med* 368(2):138–148.
5. Beer TM, et al.; PREVAIL Investigators (2014) Enzalutamide in metastatic prostate cancer before chemotherapy. *N Engl J Med* 371(5):424–433.
6. Papandreou CN, et al. (2002) Results of a phase II study with doxorubicin, etoposide, and cisplatin in patients with fully characterized small-cell carcinoma of the prostate. *J Clin Oncol* 20(14):3072–3080.
7. Aparicio AM, et al. (2013) Platinum-based chemotherapy for variant castrate-resistant prostate cancer. *Clin Cancer Res* 19(13):3621–3630.
8. Aparicio AM, et al. (2016) Combined tumor suppressor effects characterize clinically defined aggressive variant prostate cancers. *Clin Cancer Res* 22(6):1520–1530.
9. Li ZG, et al. (2008) Androgen receptor-negative human prostate cancer cells induce osteogenesis in mice through FGF9-mediated mechanisms. *J Clin Invest* 118(8):2697–2710.
10. Mandelin J, et al. (2015) Selection and identification of ligand peptides targeting a model of castrate-resistant osteogenic prostate cancer and their receptors. *Proc Natl Acad Sci USA* 112(12):3776–3781.
11. Munro S, Pelham HR (1986) An Hsp70-like protein in the ER: Identity with the 78 kd glucose-regulated protein and immunoglobulin heavy chain binding protein. *Cell* 46(2):291–300.
12. Lee AS (2014) Glucose-regulated proteins in cancer: Molecular mechanisms and therapeutic potential. *Nat Rev Cancer* 14(4):263–276.
13. Zhuang L, et al. (2009) Expression of glucose-regulated stress protein GRP78 is related to progression of melanoma. *Histopathology* 54(4):462–470.
14. Zhang J, et al. (2006) Association of elevated GRP78 expression with increased lymph node metastasis and poor prognosis in patients with gastric cancer. *Clin Exp Metastasis* 23(7-8):401–410.
15. Fernandez PM, et al. (2000) Overexpression of the glucose-regulated stress gene GRP78 in malignant but not benign human breast lesions. *Breast Cancer Res Treat* 59(1):15–26.
16. Lee E, et al. (2006) GRP78 as a novel predictor of responsiveness to chemotherapy in breast cancer. *Cancer Res* 66(16):7849–7853.
17. Miao YR, et al. (2013) Inhibition of established micrometastases by targeted drug delivery via cell surface-associated GRP78. *Clin Cancer Res* 19(8):2107–2116.
18. Daneshmand S, et al. (2007) Glucose-regulated protein GRP78 is up-regulated in prostate cancer and correlates with recurrence and survival. *Hum Pathol* 38(10): 1547–1552.
19. Pootrakul L, et al. (2006) Expression of stress response protein Grp78 is associated with the development of castration-resistant prostate cancer. *Clin Cancer Res* 12(20 Pt 1):5987–5993.
20. Tan SS, et al. (2011) GRP78 up-regulation is associated with androgen receptor status, Hsp70-Hsp90 client proteins and castrate-resistant prostate cancer. *J Pathol* 223(1):81–87.
21. Arap MA, et al. (2004) Cell surface expression of the stress response chaperone GRP78 enables tumor targeting by circulating ligands. *Cancer Cell* 6(3):275–284.
22. Hajitou A, et al. (2006) A hybrid vector for ligand-directed tumor targeting and molecular imaging. *Cell* 125(2):385–398.
23. Hajitou A, et al. (2007) Design and construction of targeted AAVP vectors for mammalian cell transduction. *Nat Protoc* 2(3):523–531.
24. Hajitou A (2010) Targeted systemic gene therapy and molecular imaging of cancer contribution of the vascular-targeted AAVP vector. *Adv Genet* 69:65–82.
25. Pranjol MZ, Hajitou A (2015) Bacteriophage-derived vectors for targeted cancer gene therapy. *Viruses* 7(1):268–284.
26. Hajitou A, et al. (2008) A preclinical model for predicting drug response in soft-tissue sarcoma with targeted AAVP molecular imaging. *Proc Natl Acad Sci USA* 105(11): 4471–4476.
27. Staquicini FI, et al. (2011) Systemic combinatorial peptide selection yields a non-canonical iron-mimicry mechanism for targeting tumors in a mouse model of human glioblastoma. *J Clin Invest* 121(1):161–173.
28. Tandle A, et al. (2009) Tumor vasculature-targeted delivery of tumor necrosis factor-alpha. *Cancer* 115(1):128–139.
29. Smith TL, et al. (2016) AAVP displaying octreotide for ligand-directed therapeutic transgene delivery in neuroendocrine tumors of the pancreas. *Proc Natl Acad Sci USA* 113(9):2466–2471.
30. Paoloni MC, et al. (2009) Launching a novel preclinical infrastructure: comparative oncology trials consortium directed therapeutic targeting of TNFalpha to cancer vasculature. *PLoS One* 4(3):e4972.
31. Cardó-Vila M, et al. (2008) A ligand peptide motif selected from a cancer patient is a receptor-interacting site within human interleukin-11. *PLoS One* 3(10):e3452.
32. Vendruscolo M, Paci E, Dobson CM, Karplus M (2001) Three key residues form a critical contact network in a protein folding transition state. *Nature* 409(6820):641–645.
33. Pasqualini R, et al. (2000) Aminopeptidase N is a receptor for tumor-homing peptides and a target for inhibiting angiogenesis. *Cancer Res* 60(3):722–727.
34. Dias-Neto E, et al. (2009) Next-generation phage display: Integrating and comparing available molecular tools to enable cost-effective high-throughput analysis. *PLoS One* 4(12):e8338.
35. Merril CR, et al. (1996) Long-circulating bacteriophage as antibacterial agents. *Proc Natl Acad Sci USA* 93(8):3188–3192.
36. Molenaar TJ, et al. (2002) Uptake and processing of modified bacteriophage M13 in mice: Implications for phage display. *Virology* 293(1):182–191.
37. Zou J, Dickerson MT, Owen NK, Landon LA, Deutscher SL (2004) Biodistribution of filamentous phage peptide libraries in mice. *Mol Biol Rep* 31(2):121–129.
38. Trepel M, et al. (2009) A heterotypic bystander effect for tumor cell killing after adeno-associated virus/phage-mediated, vascular-targeted suicide gene transfer. *Mol Cancer Ther* 8(8):2383–2391.
39. Soghomonyan S, et al. (2007) Molecular PET imaging of *HSV1-tk* reporter gene expression using [18F]FEAU. *Nat Protoc* 2(2):416–423.
40. Wan X, et al. (2014) Prostate cancer cell-stromal cell crosstalk via FGFR1 mediates antitumor activity of dovitinib in bone metastases. *Sci Transl Med* 6(252):252ra122.
41. Varkaris A, et al. (2016) Integrating murine and clinical trials with Cabozantinib to understand roles of MET and VEGFR2 as targets for growth inhibition of prostate cancer. *Clin Cancer Res* 22(1):107–121.
42. Pasqualini R, et al. (2015) Targeting the interleukin-11 receptor α in metastatic prostate cancer: A first-in-man study. *Cancer* 121(14):2411–2421.
43. Mintz PJ, et al. (2003) Fingerprinting the circulating repertoire of antibodies from cancer patients. *Nat Biotechnol* 21(1):57–63.
44. Pezaro CJ, et al. (2014) Visceral disease in castration-resistant prostate cancer. *Eur Urol* 65(2):270–273.
45. Blond-Elguindi S, et al. (1993) Affinity panning of a library of peptides displayed on bacteriophages reveals the binding specificity of BiP. *Cell* 75(4):717–728.
46. Dobroff AS, et al. (2016) Towards a transcriptome-based theranostic platform for unfavorable breast cancer phenotypes. *Proc Natl Acad Sci USA*, 10.1073/pnas.1615288113.
47. Misra UK, Payne S, Pizzo SV (2011) Ligation of prostate cancer cell surface GRP78 activates a proproliferative and antiapoptotic feedback loop: A role for secreted prostate-specific antigen. *J Biol Chem* 286(2):1248–1259.
48. Kleb B, et al. (2016) Differentially methylated genes and androgen receptor re-expression in small cell prostate carcinomas. *Epigenetics* 11(3):184–193.
49. Schindelin J, et al. (2012) Fiji: An open-source platform for biological-image analysis. *Nat Methods* 9(7):676–682.
50. Giordano RJ, Cardó-Vila M, Lahdenranta J, Pasqualini R, Arap W (2001) Biopanning and rapid analysis of selective interactive ligands. *Nat Med* 7(11):1249–1253.
51. Christianson DR, Ozawa MG, Pasqualini R, Arap W (2007) Techniques to decipher molecular diversity by phage display. *Methods Mol Biol* 357:385–406.
52. National Research Council Committee (2011) *Guide for Care and Use of Laboratory Animals*, 8th ed. (National Academies, Washington, DC).
53. Serganova I, et al. (2004) Molecular imaging of temporal dynamics and spatial heterogeneity of hypoxia-inducible factor-1 signal transduction activity in tumors in living mice. *Cancer Res* 64(17):6101–6108.
54. Ponomarev V, et al. (2007) A human-derived reporter gene for noninvasive imaging in humans: Mitochondrial thymidine kinase type 2. *J Nucl Med* 48(5):819–826.
55. Serganova I, et al. (2009) Multimodality imaging of TGFbeta signaling in breast cancer metastases. *FASEB J* 23(8):2662–2672.

Supporting Information

Ferrara et al. 10.1073/pnas.1615400113

SI Materials and Methods

Cell Lines, Reagents, and Human Specimens. The PDX model MDA-PCa-118b (9) was obtained from the Prostate Cancer Patient-derived Xenograft Program at the University of Texas M. D. Anderson Cancer Center (MDACC). Human prostate cancer-derived cell lines were purchased from the American Type Culture Collection (ATCC) and cultured in Cellgro (Mediatech), supplemented with 10% (vol/vol) heat-inactivated FBS (Invitrogen Life Technologies), penicillin, and streptomycin (all from Gibco), in a 5% CO_2 cell culture incubator at 37 °C. All cell line identities were verified by short tandem-repeat microsatellite loci analysis. Frozen stocks were generated at the time of authentication and were thawed for experiments no more than 3 mo before use. All tumor cell lines used in tissue culture were tested and documented to be free from contamination by *Mycoplasma*. The GRP78-targeting soluble peptide SNTRVAP (10), along with the corresponding controls, was custom-manufactured (PolyPeptide Laboratories) and quality-controlled to our specifications [>95% (wt/wt) purity]. Human recombinant GRP78 (Stressgen Bioreagents) and the SNTRVAP-GAPDH siRNA (Sigma-Aldrich) were obtained commercially. De-identified archival AVPC specimens were obtained from patients with small cell prostate carcinoma treated at the University of New Mexico Comprehensive Cancer Center. This study adheres to current medical ethics recommendations and guidelines on human research, and has been reviewed and approved by the Clinical Ethics Service, Institutional Biohazard Committee, Clinical Research Committee, and Institutional Review Board of the University of New Mexico Comprehensive Cancer Center.

Immunohistochemistry. Formalin-fixed paraffin-embedded (FFPE) samples from the Human Tissue Repository Core at the University of New Mexico Comprehensive Cancer Center were stained in a Ventana Discovery XT biomarker platform with standardized apparatus, reagents, and protocols provided by the manufacturer (Ventana Medical Systems). Primary anti-GRP78 rabbit monoclonal antibody (Cell Signaling Technology) was used at 1:200. Following incubation in HRP-conjugated anti-goat secondary antibody (Santa Cruz Biotechnology), signal was detected with DAB chromogenic substrate (Dako). Staining of patient samples was evaluated with standard pathology protocols, applying a four-value intensity score (0, none; 1+, weak; 2+, moderate; 3+, strong). Quantification of IHC signals in mouse tissues was obtained by color deconvolution followed by DAB^+ pixel counts with the Fiji image processing package of ImageJ (49).

Site-Directed Mutagenesis of GRP78-Targeting Phage Particles. Mutant phage particles displaying alanine-scanning variants of SNTRVAP were prepared by site-directed PCR mutagenesis as described (34). Briefly, the following oligonucleotide pair sets (Sigma-Genosys) were annealed in 10 mM Tris·HCl pH 8.0, containing 100 mM NaCl, 1 mM EDTA at 10 nM, and cloned into SfiI-digested fUSE5 vector with T4 DNA ligase (Roche):

CSNTRVAPC-forward (f): GGGCTTGTAGCAACACCCGCGTGGCGCCGTGTGGGGCCGCTG, and CSNTRVAPC-reverse (r): CGGCCCCACACGGCGCCACGCGGGTGTTGCTACAAGCCCCGT;

CANTRVAPC-f: GGGCTTGTGCGAACACCCGCGTGGCGCCGTGTGGGGCCGCTG, and CANTRVAPC-r: CGGCCCCACACGGCGCCACGCGGGTGTTCGCACAAGCCCCGT;

CSATRVAPC-f: GGGCTTGTAGCGCGACCCGCGTGGCGCCGTGTGGGGCCGCTG, and CSATRVAPC-r: CGGCCCCACACGGCGCCACGCGGGTCGCGCTACAAGCCCCGT;

CSNARVAPC-f: GGGCTTGTAGCAACGCGCGCGTGGCGCCGTGTGGGGCCGCTG, and CSNARVAPC-r: CGGCCCCACACGGCGCCACGCGCGCGTTGCTACAAGCCCCGT;

CSNTAVAPC-f: GGGCTTGTAGCAACACCGCGGTGGCGCCGTGTGGGGCCGCTG, and CSNTAVAPC-r: CGGCCCCACACGGCGCCACCGCGGTGTTGCTACAAGCCCCGT;

CSNTRAAPC-f: GGGCTTGTAGCAACACCCGCGCGGCGCCGTGTGGGGCCGCTG, and CSNTRAAPC-r: CGGCCCCACACGGCGCCGCGCGGGTGTTGCTACAAGCCCCGT;

CSNTRVGPC-f: GGGCTTGTAGCAACACCCGCGTGGGCCCGTGTGGGGCCGCTG, and CSNTRVGPC-r: CGGCCCCACACGGGCCCACGCGGGTGTTGCTACAAGCCCCGT;

CSNTRVAAC-f: GGGCTTGTAGCAACACCCGCGTGGCGGCGTGTGGGGCCGCTG, and CSNTRVAAC-r: CGGCCCCACACGCCGCCACGCGGGTGTTGCTACAAGCCCCGT.

RP78 Silencing by shRNA. Five alternative Mission shRNA sequences (Sigma-Aldrich) targeting the human GRP78 were cloned into the retroviral vector pLKO.1, and are referred to as GRP78-shRNA clones 1–5. A control vector was obtained by insertion of the sequence 5′-UUCUCCGAACGUGUCACGU-3′. Lentiviruses were produced by cotransfecting 293FT cells (Invitrogen) with each of the deriving pLKO.1 vectors combined with a packaging plasmid (MD2G) and an envelope-coding plasmid (PAX2). After 72 h, viral supernatants were collected and filtered to remove cellular debris. To silence GRP78, human prostate cancer cells were plated at 70% confluence in six-well plates and transduced with the individual GRP78-shRNA or control lentivirus, and GRP78 expression was evaluated after 48 h. To obtain stably-silenced cells, 16 h after transduction with the indicated GRP78-shRNA species, medium was replaced and transduced cells were selected in puromycin (2 μg/mL).

Design and Construction of Bifunctional (GRP78-Targeting, GRP78-Silencing) siRNA. The SNTRVAP-GRP78 siRNA conjugate was obtained by 5′-end coupling of the 3′-protected sense strand of GRP78 siRNA sequence #5 (Dharmacon) with the soluble SNTRVAP peptide through a phosphoramidate bond. The resulting conjugate was purified and desalted, followed by deprotection of both strands, annealing, and precipitation according to standard protocols. A GAPDH siRNA (Mission, Sigma-Aldrich, ID: SASI_Hs01_00140981) served as a control.

Phage Binding Assays. For protein-phage binding assays, recombinant GRP78 or BSA was immobilized on microtiter wells overnight at 4 °C (1 μg per well). Wells were blocked in PBS containing 3% (wt/vol) BSA for 2 h at room temperature, and incubated for 1 h at room temperature with 1×10^9 TU of each phage. For cell-phage binding assays with the BRASIL method (50), 1×10^6 human prostate cancer cells were incubated with 1×10^9 TU of each phage for 2 h on ice and successively collected by centrifugation. Bound phage particles were recovered by bacterial infection, purified and quantitated as described previously (51).

Western Blot. Proteins were resolved on SDS/PAGE precast gels (Bio-Rad), transferred to nitrocellulose membranes (Bio-Rad), incubated with primary anti-GRP78 (Cell Signaling Technology)

or anti–β-actin (Sigma) antibody, washed and incubated with HRP-conjugated secondary antibodies. Immunoreactive bands were visualized by enhanced chemiluminescence (ECL, Bio-Rad).

Animal Models. Six- to 8-wk-old male immunodeficient BALB/c athymic or CB17 SCID mice (Charles River Laboratory) were kept on a 12-h-light/dark cycle. Rodent chow and water were available ad libitum. DU145 xenografts were established in BALB/c athymic mice by subcutaneous injection of 1×10^6 cells. The MDA-PCa-118b PDX was propagated and maintained by subcutaneous passages in CB17 SCID mice as previously described (9). During all imaging and surgical procedures, animals were anesthetized [either isoflurane 2% (vol/vol) in oxygen or tribromoethanol, 250 mg/kg], and their temperature was maintained at 38 °C with a heat-lamp. The animal experiments reported in this paper were performed at the M. D. Anderson Cancer Center. All experimentations were conducted in full compliance with the corresponding Institutional Animal Care and Utilization Committee policies and procedures, which follows a strict current guide care and use of laboratory animals (52). Before the initiation of any animal experiments, all protocols and procedures were reviewed and approved by the local Institutional Animal Care and Utilization Committee of the organization in which the experiments were executed.

GRP78-Targeting Phage Homing in Vivo. Specific homing of GRP78-targeting phage particles was evaluated: (*i*) in mice implanted with cell surface GRP78-expressing human prostate cancer cells (in comparison with mice implanted with GRP78-silenced cells), and (*ii*) in mice implanted with cell surface GRP78-expressing human prostate cancer cells and administered intravenously (5 nmol per mouse) with control siRNA (in comparison with mice administered with the same molar dose of the SNTRVAP-GRP78 siRNA conjugate). In both experimental settings, tumor-bearing mice received an intravenous administration of 2×10^{10} TU of either SNTRVAP-displaying or control phage particles, and were perfused with PBS after 24 h, followed by collection of tumors and control organs. For phage detection and quantification, half of each tissue sample was snap-frozen in liquid nitrogen and the other half was fixed in PBS containing 10% (vol/vol) buffered formalin (pH 7.4) and paraffin-embedded. Frozen tissues were homogenized with a glass Dounce homogenizer, suspended in 1 mL DMEM supplemented with 1 mM PMSF, 20 μg/mL aprotinin, 1 μg/mL leupeptin, and washed three times in the same medium. Phage particles were detected by IHC of FFPE sections as described previously (33). Phage DNA was isolated with the DNeasy Blood and Tissue Kit (Qiagen) from frozen tissues, and amounts were determined by qPCR on a 7500 Fast Real-Time PCR System (Applied Biosystems) as described previously (34).

GRP78-Targeting AAVP-Based Theranostics: Molecular-Genetic Imaging and Targeted Therapy. Experimental protocols for the generation of AAVP-based vectors have been described in technical detail elsewhere (22; reviewed in refs. 23–25). Vectors were purified from MC1061 *Escherichia coli*, resuspended in PBS and centrifuged to remove residual debris. GRP78-targeting AAVP-containing supernatants were titrated by K91 *E. coli* infection. Mice implanted with the MDA-PCa-118b PDX received a single-dose intravenously (1×10^{11} TU per mouse) of SNTRVAP-displaying or control AAVP particles 7 d after tumor implantation. Treatment with GCV at 80 mg/kg daily intraperitoneally was initiated 5 d after vector administration and continued daily for 7 d. PET/CT imaging was performed 24 h after the last GCV dose to allow sufficient time for residual clearance of GCV by metabolism or elimination. Tumor metabolic activity was determined by administration of radiolabeled [^{18}F]-FDG followed by PET and CT scans. On the following day, *HSVtk* expression was determined in PET and CT scans acquired 2 h after intravenous administration of the radiolabeled substrate [^{18}F]-FEAU. PET scans were obtained with a microPET R4 (Concorde Microsystems), equipped with a computer-controlled positioning bed in a 10.8-cm transaxial and 8-cm axial field-of-view with no septa and operating in 3D list mode. PET/CT imaging was performed with an Inveon micro-PET/CT scanner (Siemens Preclinical Solution). PET and CT image fusion and analysis were performed with ASIPro 5.2.4.0 (Siemens Preclinical Solution). To quantify [^{18}F]-FEAU, regions of interest were drawn on digitized images, and measured values were converted from nanocurie per cubed millimeter (nCi/mm^3) to the percentage of injected dose per gram of tissue (% ID/g), as described previously (26, 39).

Supplemental Discussion: Comparison Between the [^{18}F]-FEAU and ^{124}I-FIAU Substrates. The ^{124}I-FIAU substrate used in the companion article (46) can produce low nonspecific signals because of its affinity for endogenous TK1 (nuclear) and TK2 (mitochondrial) enzymes. In contrast, the ^{18}F-FEAU used in this study has no enzymatic substrate affinity for TK1, as demonstrated by several previous studies by Gelovani's group (39, 53–55). Although FEAU has considerable affinity for TK2, the mitochondrial localization of this enzyme and very tight control of the thymidine pools inside mitochondria result in almost no uptake of FEAU, even in highly proliferative tumors (39, 53–55). In addition to these observations, ^{18}F-FEAU is expected to provide cleaner background levels of radioactivity in nontarget tissues and less whole body and individual organ radiation dose exposures than ^{124}I-FIAU, because ^{124}I has a larger fraction of high-energy spectrum emissions and longer decay half-life (~4 d) compared with ^{18}F (~2 h). We used the two different substrates in the two studies to compare their tumor selectivity. In both cases, we reached similar and specific imaging signals, with just a slight difference in the background observed. However, given the associated reasoning above, we will use ^{18}F-FEAU in future translational studies.

Statistics. Data were analyzed by two-way ANOVA corrected with Bonferroni's test (for multiple comparisons of in vivo experiments), or by Student's *t* test (for paired comparisons of in vitro experiments). Data are presented as the mean ± SEM, unless otherwise specified. *P* values of less than 0.05 were considered statistically significant. All statistical analyses were performed with the Prism software v5.01 (GraphPad Software).